The Physical Chemistry of Corrosion in a Supercritical Water-cooled Reactor

D.A. GUZONAS
Atomic Energy of Canada Limited, Chalk River Laboratories, Canada

ABSTRACT

Elucidating the relationship between coolant parameters and corrosion of materials proposed for Generation IV supercritical water-cooled reactors (SCWRs) remains a challenge. The properties of the supercritical water (SCW) coolant change significantly from core inlet (~350 °C, 25 MPa) to outlet (as high as 625 °C, 25 MPa). A mechanistic framework is required to interpret materials degradation data and predict long-term behaviour. Different corrosion mechanisms exist in high-density sub-critical/near-critical water and in low-density SCW. Understanding surface, rather than bulk, coolant chemistry is required; for example, the structure of SCW near the surface and the local oxide solubility. Oxide solubility also determines the transport of radioactive species out of the core. This paper describes the link between the physical chemistry of SCW and the corrosion of SCWR materials, including corrosion product release.

1 INTRODUCTION

The supercritical water-cooled reactor (SCWR) is one of six designs selected by the Generation IV International Forum (GIF) for further research and development with the intent of having a prototype reactor in operation around 2030. The Canadian SCWR concept [1] is a pressure-tube design with light-water coolant and a separate, low-pressure heavy-water moderator system. Each fuel channel houses a 5 m fuel assembly consisting of 62 elements filled with fuel pellets. The fuel channel is a counter-flow design; from the inlet plenum the coolant travels down a central flow tube through the centre of the fuel assembly to the bottom of the channel at a relatively constant, sub-critical temperature (~350 °C), then travels upward through the fuel elements where it is heated to 625 °C and discharges into the outlet plenum and then to the high-pressure turbine.

While a large body of information exists in the literature on the behaviour of various materials under proposed SCWR conditions [2], the focus of most studies is the metal side of the environment-metal interface. The key water chemistry issues for an SCWR have been identified elsewhere [3, 4]; this paper emphasizes the need for a comprehensive understanding of the SCW environment on corrosion processes, with a particular focus on SCW density. Most testing in support of SCWR materials selection

has been performed at constant pressure and variable temperature, leading to large changes in density over the temperature ranges studied.

It should be noted that the very important effects of irradiation on both the metal and SCW are not discussed in this paper.

2 CORROSION IN AN SCWR

2.1 In-core Environment

Water enters the Canadian SCWR core at ~350 °C and exits at 625 °C, at 25 MPa. Each fuel channel can be divided into two regions defined by the bulk fluid temperature and density; a region just downstream of the fuel string inlet with relatively constant temperature but rapidly changing density, and a region of rapidly increasing temperature and low, relatively constant density. As corrosion is a surface phenomenon, Figure 1 also shows fuel cladding surface temperatures and densities; the nominal surface coolant density is the density at the fuel cladding temperature calculated using bulk SCW properties, i.e., assuming no effect of the surface on the adjacent fluid structure. The effects of these changes in coolant density will be explored further in the next sections.

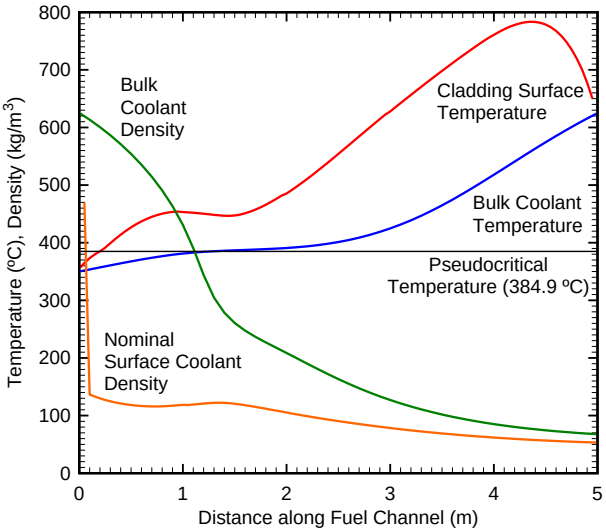

Figure 1: Bulk and surface coolant densities along the heated section of the Canadian SCWR fuel channel. The nominal surface coolant density is calculated assuming that the surface has no effect on the structure of the adjacent fluid.

2.2 Oxide Solubility

It is often assumed that the weight change (WC) of a test specimen (weight of test specimen measured before and after a test) is directly proportional to the weight loss (WL) (difference in weight of metal before and after test). The latter is proportional to the corrosion penetration and is of great practical importance. Figure 2 shows why this assumption cannot a priori be assumed true, and also illustrates the consequences of oxide dissolution from a reactor core, namely release of radioactive isotopes formed by neutron activation of alloy constituents (or corrosion products deposited in-core from the feedtrain).

The corrosion of stainless steels typically results in the formation of duplex films; an inner, typically nanocrystalline, layer, and an outer layer deposited by precipitation from solution due to oversaturation in the surface boundary layer. The growth of the outer surface film is largely determined by the transport of reactants and products through the inner film, but also depends on the extent of transport of corrosion products, released by corrosion of other parts of the system, to the surface of interest. In coolant undersaturated with respect to the solubility of the oxide phase, the outer layer can be completely dissolved [4] while in coolant supersaturated with respect to the oxide solubility, thick oxide layers can form by precipitation (Figure 3). In this example, the majority of the material in the outer oxide layer was released by corrosion of carbon steel piping at the core outlet, and transported to the core inlet by the coolant.

For a completely soluble surface oxide, WL is (Figure 2, Path a):

$$WL = (m_0 - m') \qquad \text{Equation 1}$$

If the oxide solubility is negligible, the oxides only contain metal released from base metal corrosion, and oxide have the same composition as the base metal, then WL is (Figure 2, Path b):

$$WL = WC/(1-1/f) \qquad \text{Equation 2}$$

where f is the fraction of metal in the oxide.

If the oxide solubility is low but not negligible (Figure 2, Path c), some metal released by corrosion remains in the surface oxide and some dissolves into solution. If the solution metal concentrations can be measured and metal release from the test loop or autoclave itself accounted for, the metal loss can be calculated from WC; otherwise removal of the oxide layer (descaling) is required to obtain the true corrosion rate.

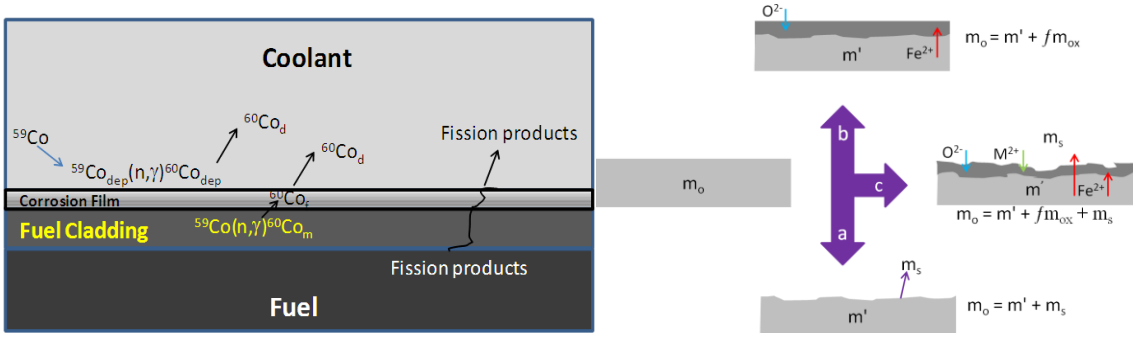

Figure 2: Right: Effect of oxide solubility on weight change. m_0 - original coupon mass; m' - mass of base material remaining after corrosion; m_{ox} - mass of oxide; m_s – mass of metal in solution; f - converts oxide mass to mass of metal. Left: Activity transport source terms [5]. Left to right: 1) deposition of corrosion products (e.g., ^{59}Co) released by feedtrain corrosion, neutron activation and then release to the coolant; 2) neutron activation in the alloy, and subsequent diffusion into the corrosion film and release to the coolant, and 3) fission product release to the coolant through a fuel defect. Subscripts indicate location: "dep" - within deposit, "d" - dissolved in coolant, "m" - within metal, and "f" - within film.

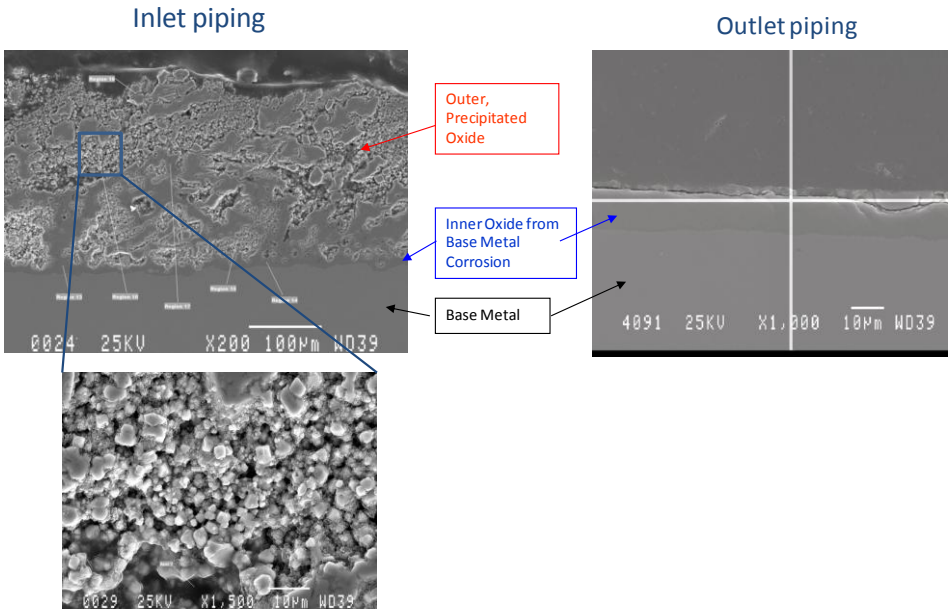

Figure 3: Cross-sections of typical deposits found on the core inlet and outlet piping of the CANDU heat transport system.

The large variations in SCW density near the critical temperature (T_c) will affect surface oxide solubility. Watanabe et al. [6] found that the WL of Ni-based alloys exposed to SCW containing 0.01 mol^{-1}·kg H_2SO_4 and 0.025 mol^{-1}·kg O_2 increased as the density increased. Guzonas et al. [7] reported that as the density of neutral pH SCW increased, the WC decreased but WL increased (Figure 4).

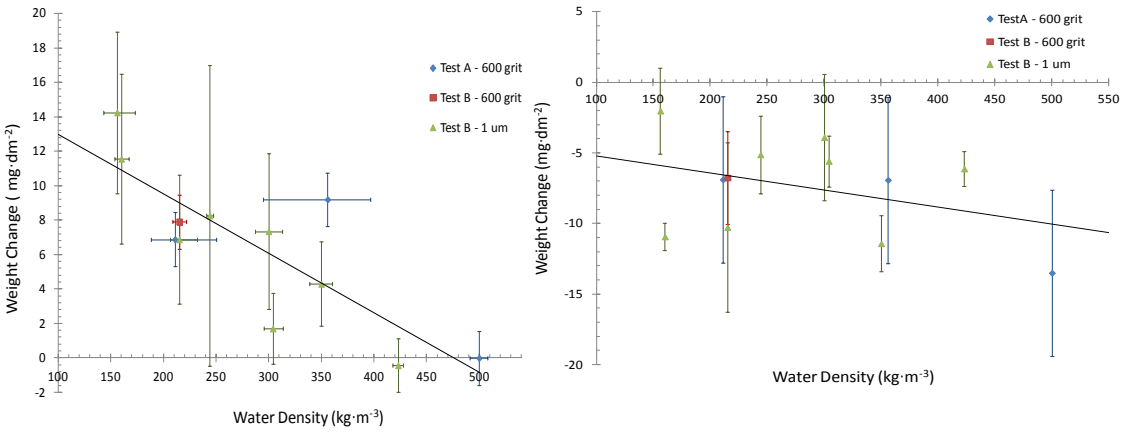

Figure 4: Average weight change (WC), left, and decaled weight loss (WL), right of 304 SS coupons exposed to SCW at 390 °C versus SCW density [7]. Vertical error bars represent the standard deviation of the average value of WC; horizontal error bars on WC data indicate the uncertainty in SCW density.

From thermodynamics it can be shown that in SCW:

$$\log(S) = \log(K_s) + n \cdot \log(\rho) \qquad \text{Equation 3}$$

where S is the oxide solubility, K_s is the equilibrium constant for the dissolution reaction, n is the number of water molecules involved in the reaction and ρ is the water density. Using the calculated solubility of magnetite as a function of pressure at 390 °C and assuming that the mass (thickness) of the outer oxide layer depends inversely on S, Equation 3 gives:

$$\log(WC) = -k \cdot \log(\rho) + C \qquad \text{Equation 4}$$

where k and C are constants. As can be seen in Figure 5 (replotted from Figure 4 data), Equation 4 gives a reasonable description of the data.

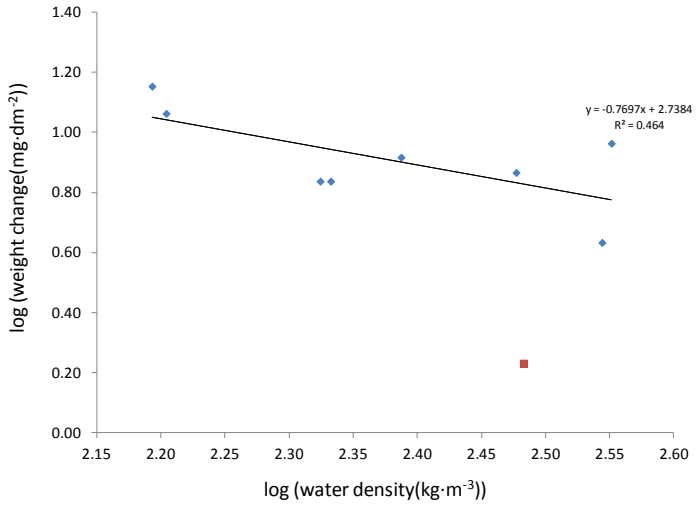

Figure 5: Log WC of 304 SS versus log SCW density [8]. The line is a linear least squares fit to the data; the datum indicated by the red square was excluded from the fit.

2.3 Corrosion on the Micro-Scale

Corrosion in sub-critical aqueous systems and high-density SCW is an electrochemical process involving distinct oxidation and reduction half-reactions that can be separated as long as there is both electronic and electrolytic contact between the anodic and cathodic sites. The low ionic conductivity of low-density SCW does not favour such separation and the corrosion mechanism becomes analogous to gas-phase oxidation. One reaction (e.g., water reduction to O^{2-}) occurs at the corrosion-film/fluid interface and the other (metal oxidation) at the metal-inner oxide layer interface.

To gain insights into the observed temperature dependence of corrosion in SCW, Guzonas and Cook [4] extended a phenomenological model proposed by Kritsunov and Macdonald [8], adding chemical oxidation (CO - direct chemical reaction) as a parallel process to the electrochemical oxidation (EO - separated cathodic and anodic sites) considered in the original model (terminology after [9]). The relative corrosion rate, R, of a metal in contact with a process stream is [4]:

$$\boldsymbol{R = k_{EO}\exp\left(-\frac{E_{EO}}{RT}\right)C_H^m C_{O_2}^n + k_{CO}\exp\left(-\frac{E_{CO}}{RT}\right)C_{O_2}^p} \qquad \text{Equation 5}$$

where k_{EO} (E_{EO}) and k_{CO} (E_{CO}) are the heterogeneous rate constants (activation energies) for the EO and CO mechanisms, respectively, T is the absolute temperature, C^n_{O2} and C^p_{O2} are the oxygen concentrations, C^m_{H+} is the hydrogen ion concentration, and m, n and p are reaction orders with respect to each component. Figure 6 shows the EO, CO components and R; the Arrhenius temperature dependence of the EO component results in a continuously increasing value of R with increasing temperature up to T_c, but the rapid drop in SCW density around the critical point decreases the availability of reactants, resulting in a drop in R. Well above T_c, R again exhibits Arrhenius temperature behaviour as the CO mechanism becomes dominant.

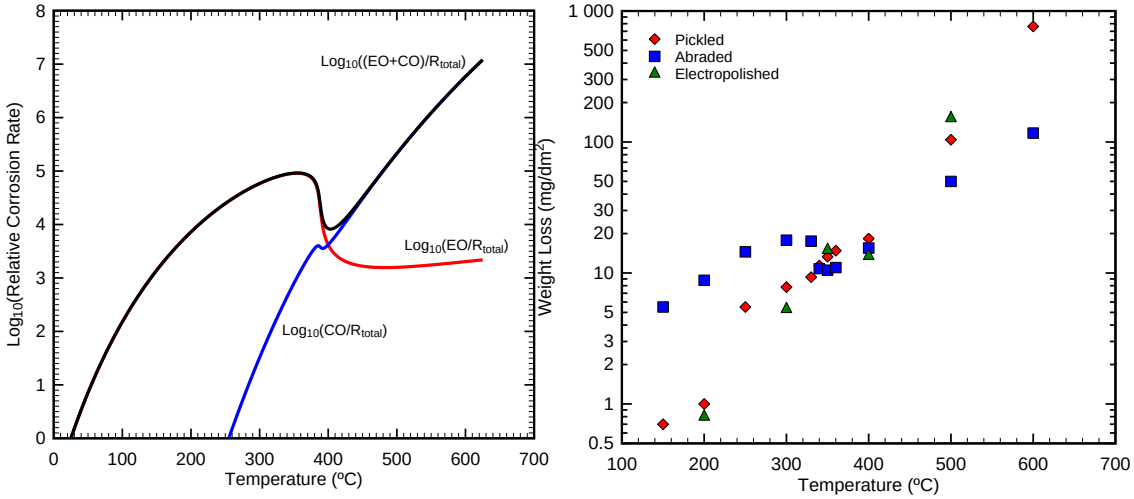

Figure 6: Predicted relative corrosion rate (left) [4] for m, n = 0.5, p = 1, pressure = 25 MPa, E_{EO} =50 kJ/mol and E_{CO} = 200 kJ/mol, and data for corrosion of 304 SS in sub-critical water and superheated steam [10] (right).

In Figure 6, data for corrosion of 304 SS in sub-critical water and superheated steam [10] are shown for comparison; an inflection near T_c, and in some cases a change in slope above and below T_c, is seen, suggesting differences in activation energy. The model and data both show a **local** maximum in the vicinity of T_c, and in this region both the EO and CO processes could occur. Guan and Macdonald [9] inferred a cut-off density for the EO mechanism of ~60 kg/m^3; the data of Liu and Macdonald [11] suggest a cut-off at ~125 kg/m^3. Recent molecular dynamics simulation studies [12] suggest a large enhancement in ion-pair dissociation at a bulk SCW density of 50 kg/m^3.

While Equation 5 provides insights into the temperature dependence of corrosion rates resulting from the changes in solvent density around T_c, it provides no insights into the kinetics of oxide formation. Recently, Penttila et al. [13] proposed a model for the formation and composition of corrosion films in SCW. They developed an equation for the change in outer oxide layer thickness, $\frac{dL_o}{dt}$:

$$\frac{dL_0}{dt} = D_{0,Fe} \cdot \frac{\Delta y_{Fe}}{L_0} \qquad \text{Equation 6}$$

where $D_{o,Fe}$ = the diffusion coefficient of Fe in the outer oxide layer, Δy_{Fe} = the change in molar fraction of Fe in the oxide, and L_o = the thickness of the outer oxide layer. To account for oxide dissolution (or precipitation from solution) we can add the expression proposed by Olive and Cook [14] for the precipitated oxide thickness:

$$\frac{dL_0}{dt} = k_{OLFe}\left(C_{O/S} - C_{sat}\right) \qquad \text{Equation 7}$$

where $\mathbf{\frac{dL_0}{dt}}$ = change in outer layer thickness, k_{OLFe} = kinetic deposition (or dissolution) constant (notation of [13]), and $C_{O/S}$ and C_{sat} = oxide solution and saturation concentrations, respectively. From Equation 3, $C_{sat} = K_s \cdot \rho^n$, substituting into Equation 7 and combining Equations 6 and 7 gives:

$$\frac{dL_0}{dt} = D_{0,Fe} \cdot \frac{\Delta y_{Fe}}{L_0} + k_{OLFe}\left(C_{O/S} - K_s \cdot \rho^n\right) \qquad \text{Equation 8}$$

This approach is similar to that taken by MacDonald [15] to model the effect of dissolution on the **passive** (inner) layer thickness. When $C_{O/S}$ is small, e.g., flow loop with low impurity concentrations at the test section inlet, the oxide thickness will depend on the SCW density. In low-density SCW, the oxide thickness will be dominated by the first term in Equation 8 unless the oxide solubility is high, and weight gain will be a reasonable measure of the corrosion rate unless there is oxide spalling. Equation 8 also introduces the possibility of adding a flow rate dependence.

2.4 Corrosion on the Nanoscale

Having established that SCW density plays an important role in corrosion in SCW, one must ask the question "What is the relevant SCW density?" As the SCW density decreases the surface water structure must change from that of an electrical double layer to one in which only clusters of adsorbed water exist at the surface (Figure 7). At high SCW density, the overall corrosion reaction consists of oxidation and reduction half-reactions. Electrons are transported in the metal, while the charge imbalance in solution resulting from production or consumption of ions is balanced by ion transport through the solution. For simplicity it is assumed that the solubility of the metal oxide(s) produced is high and no protective oxide film forms.

In the "transition region" discrete anodic and cathodic sites may still exist, but are closer together, as ion pairs become the favoured solution species and the charge balance in solution must be more localized. The large density fluctuations that occur in the near-critical region in the bulk water are expected to exist at the surface as well, and a continuous, stable double layer may not exist over the entire surface.

In low-density SCW (T> 500 °C) ionic species are not favoured, metal oxide solubility is low, and corrosion occurs via the inward and outward vacancy diffusion (CO mechanism). Water exists on the surface as small clusters of 'liquid-like' water separated by regions of 'gas-like' water.

Guzonas and Cook [4] suggested that the SCW structure directly adjacent to a surface would differ from that of the bulk fluid, being more organised with a somewhat higher density, in the same way that the local SCW structure around ions is different than that of bulk SCW [16]. Thus, a continuous, liquid-like film may persist at the surface at temperatures well above T_c. This change in structure at the surface is implied in the 'transition region' shown in Figure 7, where gas-like properties may not be fully realized due to the imposition of liquid-like densities at the surface. To confirm this hypothesis, Svishchev et al. [17] recently performed MD calculations that show that a higher-density surface region is predicted at a model surface, $Fe(OH)_2$ (Figure 7 right hand side).

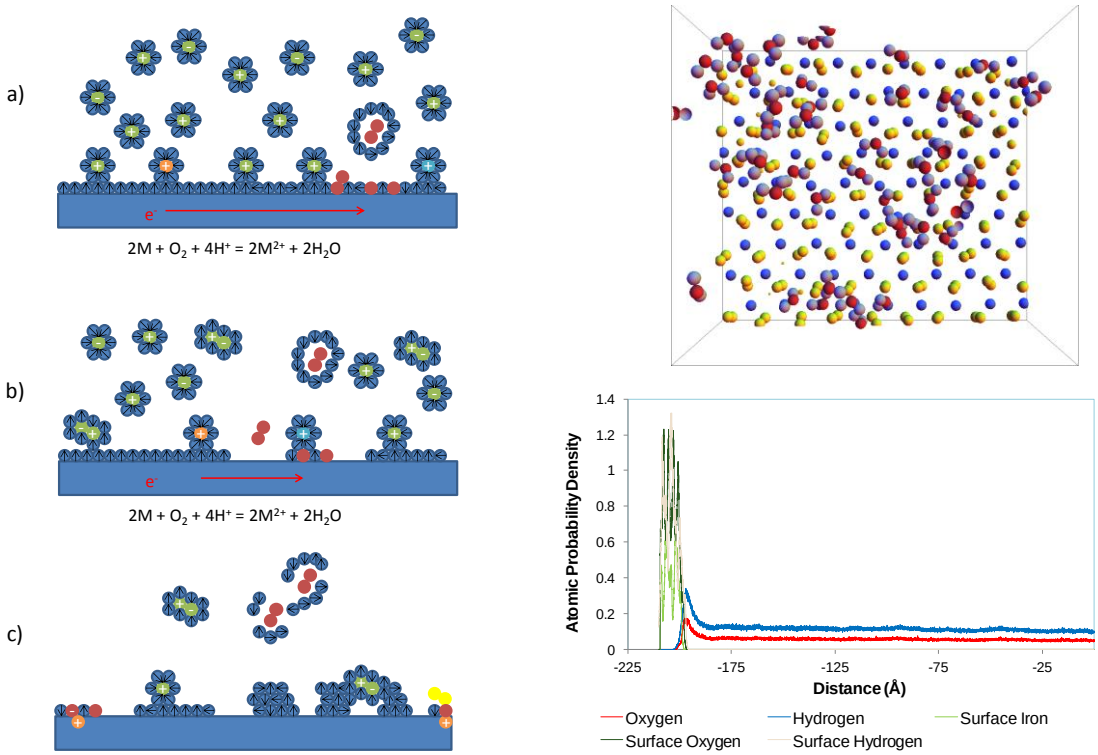

Figure 7: Left – Schematic illustrating possible structures of water adjacent to a metal surface [4]: Left a) subcritical water with electric double layer; b) transition region; c) gas-phase oxidation with surface clustering. Right- typical configuration of water molecules and atomic density distributions at $Fe(OH)_2$ – SCW interface, SPC/E water model, T = 715 K, bulk water density = 0.075 g/cc [17].

3 SUMMARY

This paper has argued that SCW density is a key factor often neglected in testing for SCWR materials selection, but which plays a major role in determining the weight change of test coupons. This is particularly true at temperatures near T_c. Bischoff [18], Motta et al. [19] and Guzonas and Cook [4] have highlighted the similarity between

corrosion in SCW at 25 MPa SCW and in steam at $T>>T_c$ (i.e., low-density SCW), the weight gain being slightly higher at the higher pressure. Under these conditions oxide solubility plays a small role in determining the thickness of the outer oxide layer. This suggests that a reasonable assessment of materials behaviour under SCWR conditions above 500 °C can be obtained using measurements in low pressure steam; these experiments can be much simpler than those using SCW above the critical pressure.

Typical schematics of corrosion processes at a surface in SCW usually consider the alloy, an inner oxide layer, an outer oxide layer, and SCW, with the implied admonition seemingly being "hic sunt dracones". Figure 8 suggests a slightly more 'realistic' view, with bulk SCW, an ordered region adjacent to the surface, and a very thin interfacial region where oxide and solvent intermix; Svishchev et al. [17] reported a small shoulder in the water oxygen density profile that suggested that a small number of adsorbed water molecules penetrate further into the surface up to a distance of about 2 Å. Consideration of the SCW environment will improve our ability to predict the effects of coolant flow, oxidant concentration and to better interpret experimental data.

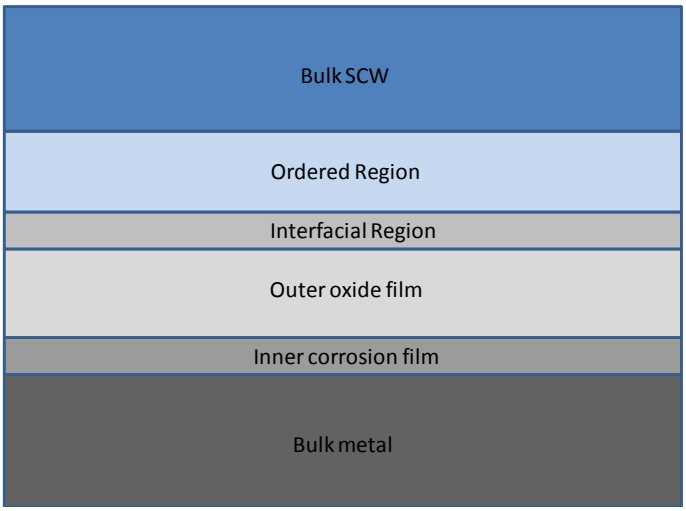

Figure 8: A more realistic depiction of the metal-SCW interface.

REFERENCE LIST

[1] M. Yetisir, M. Gaudet and D. Rhodes, "Development and Integration of Canadian SCWR Concept with Counter-Flow Fuel Assembly", ISSCWR-6, March 03-07, 2013, Shenzhen, Guangdong, China.

[2] T. Allen, Y. Chen, D.A. Guzonas, X. Ren, K. Sridharan, L. Tan, G. Was and E. West, "Material Performance in Supercritical Water", in: R. Konings (Ed.), Comprehensive Nuclear Materials, Elsevier, 2012.

[3] D.A. Guzonas, P. Tremaine, F. Brosseau, J. Meesungnoen and J.-P. Jay-Gerin, "Key Water Chemistry Issues in a Supercritical-Water-Cooled Pressure-Tube Reactor", Nucl. Technology, **179** (2012) 205.

[4] D.A. Guzonas and W.G. Cook, "Cycle Chemistry and Its Effect on Materials in a Supercritical Water-Cooled Reactor: A Synthesis of Current Understanding", Corrosion Science, **65** (2012) 48.

[5] D.A. Guzonas and L. Qiu, "Activity Transport in a Supercritical Water-Cooled Reactor", 6th International Symposium on Supercritical Water-Cooled Reactors, March 03-07, 2013, Shenzhen, Guangdong, China.

[6] Y. Watanabe, Y. Daigo, K. Sue and T. Adschiri, "Characteristics and a Few Key Parameters of Corrosion of Alloys in Supercritical Water Environments", Transactions of the Indian Institute of Metals. 56 (2003) 297-304.

[7] D.A. Guzonas, K. Bissonette, L. Deschenes, H. Dole and W. Cook, "Mechanistic Aspects of Corrosion in a Supercritical Water-Cooled Reactor", 6th Int. Symp. on Supercritical Water-Cooled Reactors, Shenzhen, Guangdong, China, March 03-07, 2013.

[8] L.B. Kriksunov and D.D. Macdonald, "Corrosion in Supercritical Water Oxidation Systems: A Phenomenological Analysis, J. Electrochem. Soc. **142** (1995) 4069-4073.

[9] X. Guan and D.D. Macdonald, "Determination of Corrosion Mechanisms and Estimation of Electrochemical Kinetics of Metal Corrosion in High Subcritical and Supercritical Aqueous Systems, Corrosion. **65** (2009) 376-387.

[10] T. Maekawa, M. Kagawa and N. Nakajima, "Corrosion Behaviours of Stainless Steel in High-Temperature Water and Superheated Steam, Transactions of the Japan Institute of Metals. **9** (1968) 130-136.

[11] C. Liu and D.D. Macdonald, "An Advanced Pd/Pt Relative Resistance Sensor for the Continuous Monitoring of Dissolved Hydrogen in Aqueous Systems at High Subcritical and Supercritical Temperatures, The Journal of Supercritical Fluids. 8 (1995) 263-270.

[12] A.A. Chialvo, M.S. Gruszkiewicz and D.R. Cole, "Ion-Pair Association in Ultrasupercritical Aqueous Environments: Successful Interplay among Conductance Experiments, Theory, and Molecular Simulations", J. Chem. Eng. Data. **55** (2010) 1828-1836.

[13] S. Penttila, I. Betova, M. Bojinov, P. Kunnunen and A. Toivonen "Estimation of Kinetic Parameters of the Corrosion Layer Constituents on Steel in Supercritical Water Coolant", Corrosion Science **53** (2011) 4193.

[14] W.G. Cook and R.P. Olive, "Prediction of Crud Deposition in a CANDU-SCWR Core through Corrosion Product Solubility and Transport Modelling", Proceedings of the 5th International Symposium on Supercritical Water-Cooled Reactors, Vancouver, BC, Canada, (2011).

[15] D.D. MacDonald, "Passivity – The Key to our Metals-Based Civilization", Pure Appl. Chem. **71** (1999) 951.

[16] S.C. Tucker, "Solvent Density Inhomogeneities in Supercritical Fluids", Chem. Rev. **99** (1999) 391-418.

[17] I.M. Svishchev, D.T. Kallikragas and A.Yu. Plugatyr, "Molecular Dynamics Simulations of Supercritical Water at the Iron Hydroxide Surface", J. of Supercritical Fluids **78** (2013) 7– 11.

[18] J. Bischoff, "Oxidation Behaviour of Ferritic-Martensitic and ODS Steels in Supercritical Water, Dissertation in Nuclear Engineering, The Pennsylvania State University, Department of Mechanical and Nuclear Engineering (2011).

[19] A.T. Motta, A. Yilmazbayhan, da Silva, Marcelo J. Gomes, R.J. Comstock, G.S. Was, J.T. Busby, E. Gartner, Q. Peng, Y.H. Jeong and J.Y. Park, "Zirconium Alloys for Supercritical Water Reactor Applications: Challenges and Possibilities", J. Nucl. Mater. **371** (2007) 61-75.